Experimental Investigation of Light-Gauge Steel Plate Shear Walls

Jeffrey W. Berman[1] and Michel Bruneau[2]

Abstract: This paper describes the prototype design, specimen design, experimental setup, and experimental results of three light-gauge steel plate shear wall concepts. Prototype light-gauge steel plate shear walls are designed as seismic retrofits for a hospital structure in an area of high seismicity, and emphasis is placed on minimizing their impact on the existing framing. Three single-story test specimens are designed using these prototypes as a basis, two specimens with flat infill plates (thicknesses of 0.9 mm) and a third using a corrugated infill plate (thickness of 0.7 mm). Connection of the infill plates to the boundary frames is achieved through the use of bolts in combination with industrial strength epoxy or welds, allowing for mobility of the infills if desired. Testing of the systems is done under quasi-static conditions. It is shown that one of the flat infill plate specimens, as well as the specimen utilizing a corrugated infill plate, achieve significant ductility and energy dissipation while minimizing the demands placed on the surrounding framing. Experimental results are compared to monotonic pushover predictions from computer analysis using a simple model and good agreement is observed.

DOI: 10.1061/(ASCE)0733-9445(2005)131:2(259)

CE Database subject headings: Shear walls; Experimentation; Retrofitting; Seismic design; Cyclic design; Steel plates.

Introduction

Past research on steel plate shear walls (SPSW) has investigated the use of flat hot-rolled plates as infill panels. By allowing the infill plates to buckle in shear, develop diagonal tension field action, and then dissipate energy through the cyclic yielding of the infill in tension, researchers have shown that SPSWs can be a useful seismic energy dissipation system (Thorburn et al. 1983; Timler and Kulak 1983; Caccese et al. 1993; Elgaaly et al. 1993; Driver et al. 1997; Rezai 1999; etc.). Such research has also produced useful analytical models for representing SPSWs that are allowed to develop tension field action, and some of these have been implemented in a steel design standard [Canadian Standards Association (CSA) 2001]. However, use of SPSWs with hot-rolled infill plates (typically 5 mm, 3/16 in., minimum thickness) in a retrofit situation, in which it would be used to infill an existing bay, would likely require significant reinforcement of the existing beams and columns due to the large demands induced from the plate yielding.

Light-gauge SPSWs could provide engineers with an effective option for the seismic retrofit of older buildings. The concept is to create a system that is strong enough to resist the necessary seismic forces, and yet light enough to avoid having to heavily reinforce existing framing due to the increased demands the retrofit strategy may place on it. Furthermore, an interest exists in creating systems that could be installed with minimum disruption to the function and occupants of an existing building, and, in the context of the seismic retrofit of hospitals, that could be modular to facilitate relocation of the light-gauge infills as floor plans are rearranged (something that often occurs in hospitals). This paper describes the design and quasi-static testing of three such light-gauge SPSW systems.

Prototype Design

Two prototype light-gauge steel plate shear walls were designed as seismic retrofit options for a prototype demonstration hospital (Yang and Whittaker 2002). This hospital is a four-story steel framed building with plan dimensions of 83.5 m (274 ft) in the east–west direction and 17.2 m (56.4 ft) in the north–south direction. The floor plan is shown in Fig. 1. The first story has a height of 4.1 m (13.5 ft) and the others are 3.8 m high (12.5 ft). Gravity framing consists of 140 mm (5.5 in.) thick reinforced concrete floor slabs on steel deck that rest on steel floor beams and girders which carry the gravity loads to columns. In the north–south direction (the direction of interest here), there are four moment-resisting three-bay frames that act as the primary lateral load resisting system (located on frame lines B, H, J, and N). The remaining frames (termed gravity frames) in the north–south direction utilize flexible web–angle connections that are assumed to have no resistance to lateral loading. Yang and Whittaker (2002) describe several sets of steel section sizes meant to represent hospitals constructed in different time periods and locations, therefore, satisfying different building code requirements. The design representing a typical hospital constructed on the west coast in the 1960s (WC60) was used in this study. The test specimens were designed to retrofit the north–south frames and they included the flexible web–angle beam-to-column connections. To minimize the

[1]PhD Candidate, Dept. of Civil, Structural and Environmental Engineering, Univ. at Buffalo, Amherst, NY 14260. E-mail: jwberman@eng.buffalo.edu

[2]Deputy Director, Multidisciplinary Center for Earthquake Engineering Research, Professor, Dept. of Civil Structural and Environmental Engineering, Univ. at Buffalo, Buffalo, NY 14260-4300.

Note. Associate Editor: Christopher J. Earls. Discussion open until July 1, 2005. Separate discussions must be submitted for individual papers. To extend the closing date by one month, a written request must be filed with the ASCE Managing Editor. The manuscript for this paper was submitted for review and possible publication on March 25, 2003; approved on May 11, 2004. This paper is part of the ***Journal of Structural Engineering***, Vol. 131, No. 2, February 1, 2005. ©ASCE, ISSN 0733-9445/2005/2-259–267/$25.00.

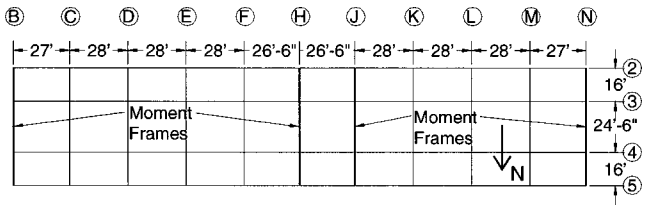

Fig. 1. Demonstration hospital floor plan (Adapted from Yang and Whittaker 2002)

forces applied to the existing framing by the yielding infill plates (i.e., to avoid having to strengthen the existing columns), it was decided that every line of gravity framing in the north–south direction would be retrofitted. The middle bay (between framing lines 3 and 4) was arbitrarily chosen as the location for the retrofit on each frame line. This choice may restrict access and cause serviceability issues that would have to be considered in implementation.

The equivalent lateral force procedure of Federal Emergency Management Agency (FEMA) Document, FEMA 302 (FEMA 1997), was used to calculate a design base shear. Tributary gravity loads for one bay of north–south framing were determined. These and a portion of the design live load were used as the active seismic weight for a single-gravity frame line. The hospital was assumed to be located in Northridge, California on a class D soil. Because a SPSW is not a structural system covered by FEMA 302, a seismic force reduction factor, R, was derived from the SPSW design provisions of the Canadian Steel Design Standard, CAN/CSA-S16-01 (CSA 2001). For a limited ductility SPSW (i.e., SPSW in frames with simple beam-to-column connections), the CSA requirements would be equivalent to an R of 3.33 for use in FEMA 302, which was used for calculation of the base shear. An importance factor, I, of 1.5 was used because this is considered a critical facility. The resulting seismic coefficient, C_s, was determined to be 0.58 and the corresponding base shear tributary to one of the gravity frames was approximately 1,420 kN (320 kips). Note that the calculation of base shear applied to one of the gravity frames neglected the stiffness of the existing moment frames (they were assumed to have a small stiffness relative to the infilled gravity frames) as well as the effect of torsional response in plan, but still provides a reasonable basis to develop plate sizes for the purpose of this study.

For the calculated design base shear, plate thicknesses for both flat and corrugated plate specimens were found using the procedure described in Berman and Bruneau (2003b). This procedure is based on development of the plastic collapse mechanisms for the strip model illustrated in Fig. 2, that was formulated by Timler and Kulak (1983) and implemented in CAN/CSA-S16-01 (CSA 2001). Minimum required plate thicknesses at the first floor level were found to be 22 Gauge (0.75 mm or 0.0295 in.) for the corrugated infill plate, and 20 Gauge (1.0 mm or 0.0396 in.) for the flat infill plates. A yield stress of 380 MPa (55 ksi) was assumed in both cases. A Type B steel deck, as illustrated in Fig. 3, with the corrugations orientated at 45° from the horizontal was assumed above, and the required plate thickness was calculated using a modified version of the design equation in Berman and Bruneau (2003b), namely,

$$t = \frac{2V}{R_c F_y L \sin 2\alpha} \tag{1}$$

where V=story shear force; R_c=ratio of one wavelength of corrugation, ℓ_w, to the projected flat length of one corrugation, ℓ_p, as

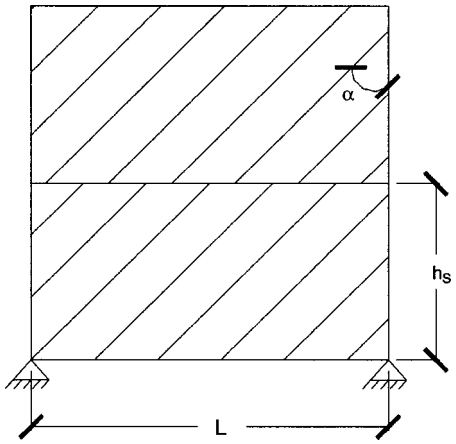

Fig. 2. Strip model

shown in Fig. 3; L=bay width; and α=angle of inclination of the strips as shown in Fig. 2 (taken as 45° for the corrugated infill to match the orientation of the tension field calculated for the flat infills). Note that tension field action can only develop in the direction parallel to the corrugations, and that pairs of retrofitted bays (with corrugations oriented in opposite directions) are required to implement this system. The corrugated infills were also orientated with the ribs at 45° because the additional compression resistance they provide was thought to be a possible advantage. Eq. (1) with R_c equal to 1.0 was used to calculate the needed thickness of the flat infills.

Test Specimen Design

Using the prototype designs as a basis, three light-gauge SPSW specimens (two flat infill plate specimens with different infill-to-boundary frame connections, and one corrugated specimen) were designed for quasi-static testing in the Structural Engineering and Earthquake Simulation Laboratory (SEESL) at the University at Buffalo. The infill plate thicknesses for the specimens were selected to be identical to those for the prototype retrofits for the demonstration hospital. This was done to maintain practical plate gauge thicknesses. However, the maximum force available for quasi-static testing using a single actuator in the SEESL is 1,110 kN (250 kips). Therefore, the bay width was scaled down from the prototype, as this parameter, aside from yield stress and plate thickness, determines the ultimate strength of SPSWs in single-story frames having simple beam-to-column connections. The 2:1 (L:h) aspect ratio of the prototype was also maintained for the specimens. The bay width and story height of the specimens were designed to be 3,660 mm (12 ft) and 1,830 mm (6 ft), respectively (i.e., approximately $\frac{1}{2}$ scale from the prototypes).

Ultimate strengths of specimens having the same plate thicknesses determined above were estimated to be 710 kN (160 kips)

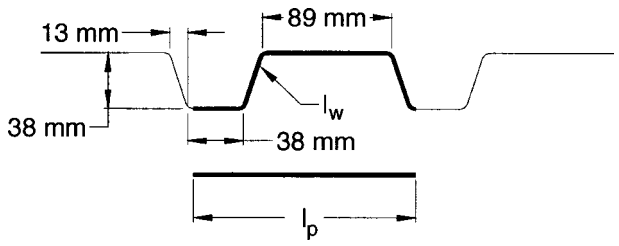

Fig. 3. Corrugation pattern of Type B steel deck

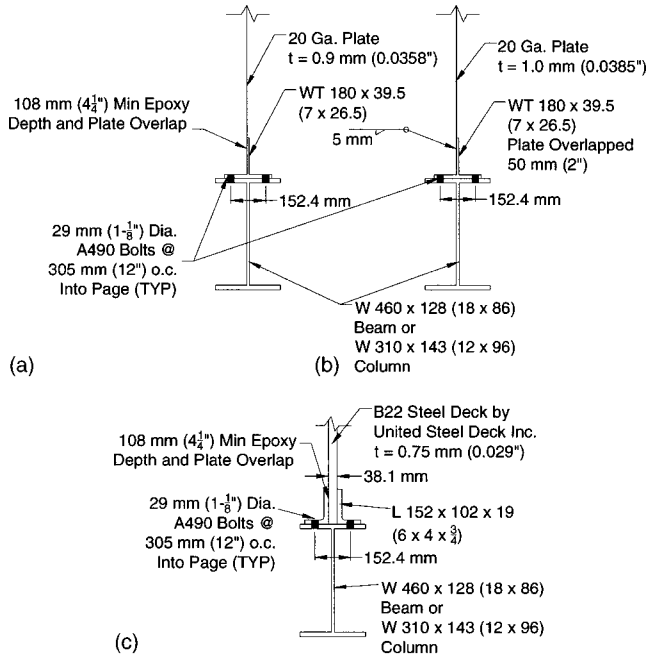

Fig. 4. Infill-to-boundary frame connections (a) Specimen F1 (b) Specimen F2 (c) Specimen C1

and 645 kN (145 kips) for the corrugated and flat infills, respectively [using a yield stress 380 MPa (55 ksi) for each], neglecting the contribution of the web–angle beam-to-column flexible connections in the boundary frame. Resulting slenderness ratios (L/t) were 4,880 and 3,636, respectively, for the corrugated and flat infill plates.

Strip models of each specimen using a yield stress of 380 MPa (55 ksi) for the infill material were developed and, using the results of pushover analyses, boundary frames for the infills were designed to remain elastic with a safety factor of 2.5, resulting in $W\,310\times143$ (US-$W\,12\times96$) columns and $W\,460\times128$ (US-$W\,12\times86$) beams. The beam-to-column connections using $L\,203\times102\times12.7$ $\left(\text{US-}L\,8\times4\times\frac{1}{2}\right)$ angles on both sides of the beam web were welded to the beam and bolted to the column flanges.

Connecting the infill plates to the surrounding frame members proved difficult and a number of different options were explored, some of which are detailed in Berman and Bruneau (2003a). In the case of the flat infills, two alternatives were developed for Specimens F1 and F2 as illustrated in Figs. 4(a and b). The connection for Specimen F1 relied on industrial strength epoxy (Loctite 2001), which was determined to have a lap shear strength of approximately 17.2 MPa (2.5 ksi) and a handling time of roughly 30 min. Details about how this epoxy was selected and how the 108 mm length of overlap shown in Fig. 4 was obtained are given in Berman and Bruneau (2003a). The infill plate was fully welded for Specimen F2. In both cases, the infill was attached to intermediate $WT\,180\times39.5$ (US-$WT\,7\times26.5$) sections that were then bolted to the boundary frame to model a connection detail that would allow possible future relocation of the infill. To test the effectiveness of SPSW with corrugated infills, Specimen C1 was developed, in which the corrugated infill was connected to the boundary frame using the epoxy and intermediate $L\,152\times102\times19$ (US-$L\,6\times4\times3/4$) as shown in Fig. 4(c). Due to the fact that corrugated metal deck is available in only 910 mm (3 ft) or 610 mm (2 ft) widths, the infill of Specimen C1 was made up of

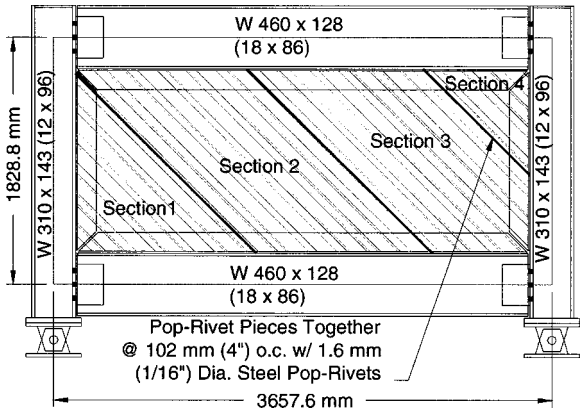

Fig. 5. Sections of infill of Specimen C1

four sections as shown in Fig. 5. These sections were connected to each other using 1.6 mm (1/16 in.) diameter steel pop rivets spaced at 100 mm (4 in.) on center.

The test setup is shown in Fig. 6. Specimens are mounted on large clevises attached to a foundation beam, itself tensioned to the strong floor of the SEESL. Lateral load was applied at the top of the wall by a servocontrolled hydraulic actuator mounted between the specimen and a reaction frame. The recommended Applied Technology Council (ATC) loading protocol of ATC 24 (ATC 1992) was followed. Table 1 shows the displacement history for each specimen and Figs. 7(a and b) show Specimens F1 and C1 prior to testing.

Coupon tests of the infill material were performed and the resulting stress–strain curves are shown in Figs. 8(a–c). Yield stresses of 152, 214, and 330 MPa were obtained for specimens F1, F2, and C1. The material for specimens F1 and F2 was ASTM A1008, which is a cold-rolled, carbon, commercial steel sheet with no mandatory mechanical properties. ASTM states that typical yield stresses are between 140 MPa and 275 MPa (20 and 40 ksi) and elongations at fracture of 20% in 50 mm (2 in.) (ASTM 1997). The material for specimen C1 was ASTM A653 Grade 33, which is a galvanized material with a minimum yield stress of 230 MPa (33 ksi) and a minimum elongation at fracture of 20% in 50 mm (2 in.) (ASTM 1998). Measured thicknesses of the infills were 0.91, 0.98, and 0.75 mm (0.0358, 0.0386, and 0.0295 in.) for specimens F1, F2, and C1, respectively. Coupon tests of the boundary frames were not performed because the boundary frames were expected to remain elastic, but the material was specified to be ASTM A572 Grade 50.

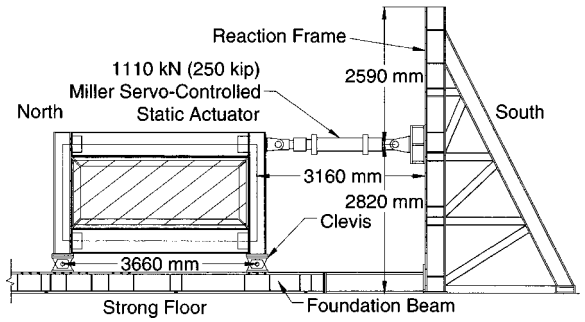

Fig. 6. Test setup

Table 1. Cyclic Displacement Histories

Displacement step	Number of cycles	Cumulative number of cycles	Displacement Δ/Δ_y	Displacement (mm)	Drift (%)
Specimen F1					
1	3	3	0.25	1.3	0.07
2	3	6	0.4	2.0	0.11
3	1	7	1	5.1	0.25
Specimen C1					
1	3	3	0.17	1.4	0.08
2	3	6	0.42	3.4	0.19
3	3	9	0.70	5.7	0.31
4	3	12	1	8.1	0.44
5	3	15	2	16.5	0.90
6	3	18	3	25.0	1.38
7	1.5	19.5	4	33.5	1.83
Specimen F2					
1	3	3	0.25	1.3	0.07
2	3	6	0.64	3.4	0.19
3	3	9	1	5.3	0.29
4	3	12	2	10.7	0.58
5	3	15	3	16.5	0.90
6	2	17	4	22.1	1.21
7	2	19	5	28.0	1.53
8	2	21	6	33.3	1.82
9	2	23	7	39.0	2.13
10	2	25	8	44.6	2.44
11	2	27	10	56.2	3.07
12	4	31	12	67.0	3.65

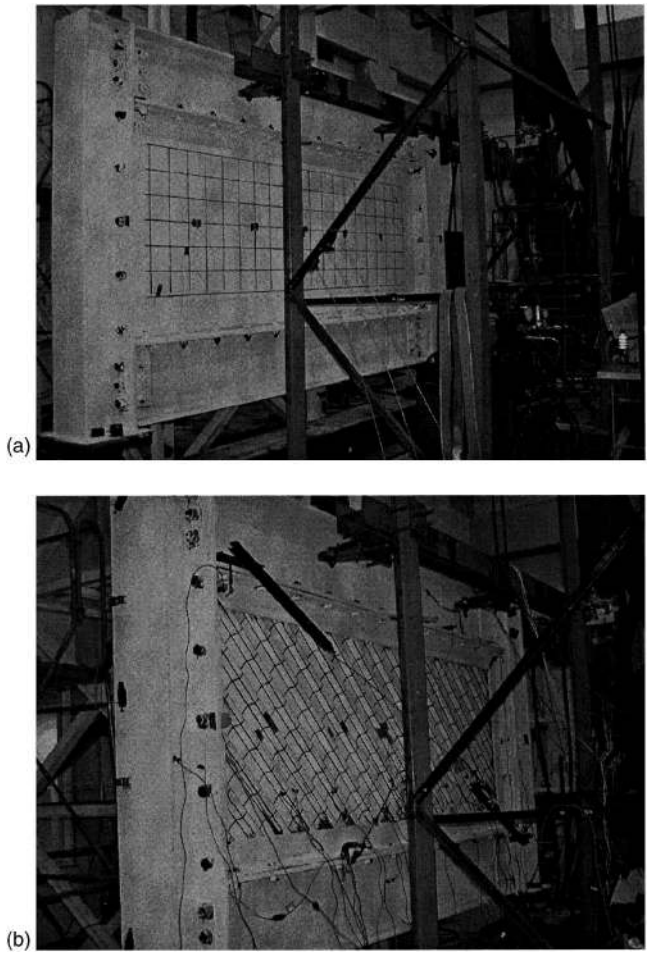

Fig. 7. Specimens prior to testing: (a) Specimen F1 and (b) Specimen C1

Experimental Results

Specimen F1

Despite the numerous ancillary tests that were performed to select an adequate connection configuration and epoxy, Specimen F1 suffered a premature failure of the epoxy during Cycle 7 at 0.25% drift while still exhibiting elastic behavior. The epoxy failed in the connection along the top beam of the specimen, and the poor epoxy coverage is shown in Fig. 9. Epoxy was directly applied to the infill plate only and not to the *WT*'s, which could have contributed to cause this insufficient coverage. Qualitatively, this hypothesis was verified by the successful testing of Specimen C1, in which epoxy was applied to both the infill plate and intermediate angles. Quantitative results on the response measured for Specimen F1 are presented in Table 2.

Specimen C1

The hysteresis curves for Specimen C1 are shown in Fig. 10(a) along with the monotonic pushover curve obtained from a strip model of the specimen using the measured material properties. Quantitative values of displacement ductility ratio, μ, and other key hysteretic response parameters are presented in Table 2. As shown, Specimen C1 reached a μ of 3 prior to losing substantial strength. Contribution of the infill to the total initial stiffness exceeded 90%. As expected, tension field action developed only in the direction parallel to the corrugations, resulting in unsymmetric hysteresis loops. Pinching of the hysteresis due to permanent plastic deformations of the infill is also apparent. This hysteretic behavior is similar to that of a braced frame with a single slender brace (Bruneau et al. 1997) and the additional strength provided by the compression of the corrugations was not observed after buckling occurred.

Following the cycles at three times yield the yield displacement, $3\Delta_y$ at 1.4% drift, Specimen C1 suffered a rapid loss in strength as is shown on the positive drift side of Fig. 10(a). This was due to infill plate fractures that occurred at locations of repeated local buckling which developed on the corrugated profile of the specimen. The buckling occurred as the specimen was loaded in the negative drift direction, which put the corrugations in compression. An example of the buckling at $-3\Delta_y$ is shown in Fig. 11 and examples of the fractures at $4\Delta_y$ are shown in Fig. 12. At the end of the test, there were three such areas of infill fractures.

The epoxy connection of the infill plate to the boundary frame of specimen C1 cracked in some locations; however, according to strain gauge data the entire plate yielded. This shows that epoxy connections are capable of developing the yield forces in thin steel plates, although more research is needed to determine the reliability of such connections.

Specimen F2

Stable and ductile behavior was observed in Specimen F2 as shown by the hysteresis loops of Fig. 10(b). Also shown in Fig.

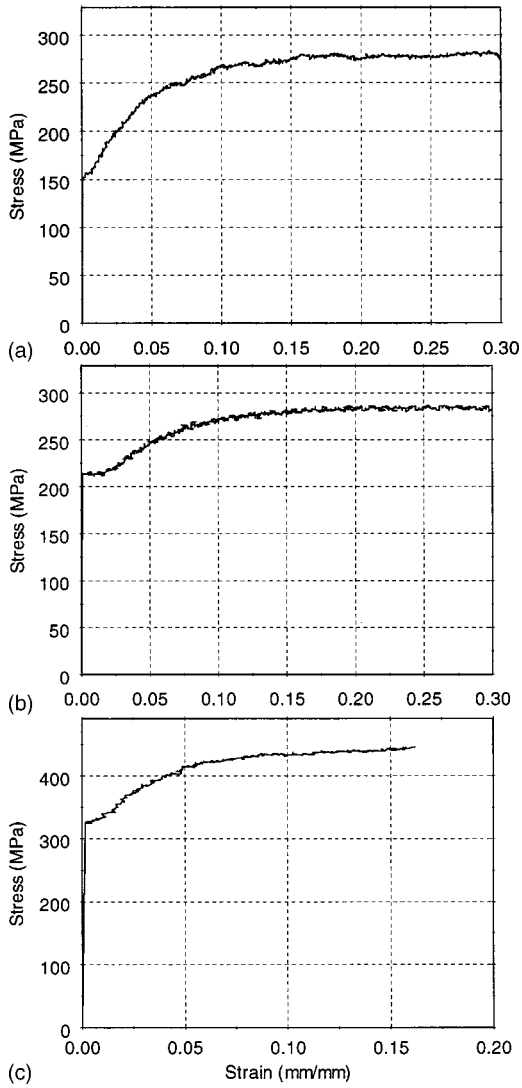

Fig. 8. Infill coupon test results (a) Specimen F1 (b) Specimen F2 (c) Specimen C1

10(b) is the monotonic pushover curve obtained from a strip model of the specimen. Reasonable agreement in terms of initial stiffness and yield base shear are evident. Specimen F2 reached a ductility ratio of 12 and drift of 3.7%, as shown in Table 2, prior to losing significant strength. Additionally, from the data presented in Table 2, the infill of Specimen F2 contributed approximately 90% of the initial stiffness of the system. The pinching exhibited by the hysteresis loops of Fig. 10(b) is again due to the accumulation of nonrecoverable plastic strains, a hysteretic behavior comparable to that of a concentrically braced frame having slender braces. Fig. 13 shows the buckling of the infill plate at the peak displacement of cycle 20 ($6\Delta_y$), and the residual buckling observed after unloading from that displacement.

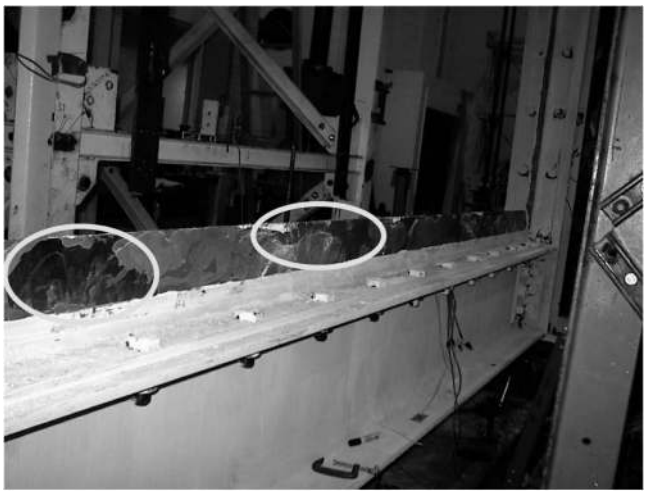

Fig. 9. Poor epoxy coverage (Specimen F1)

Ultimate failure of Specimen F2 was due to fractures that propagated from the endpoint of the welds that connected the infill to the intermediate *WT*'s. The progression of the fracture in the lower south corner of the infill is shown in Fig. 14. Similar fractures and propagation were observed in all four corners of the infill.

Boundary Frame Modeling

To further assess the adequacy of the light-gauge infills as seismic retrofit alternatives, it is necessary to separate the infill behavior from the boundary frame behavior. To do this, it is necessary to model the hysteretic behavior of the bare-boundary frame, using results of bare-boundary frame testing to calibrate the model. The results of that model can then be numerically subtracted from the experimental data.

Cook (1983) and Goto et al. (1991) used the bounding surface model with internal variables, originally formulated by Dafalias and Popov (1976), to represent the hysteretic behavior of semi-rigid frames. A summary of the model and how it is applied is given in Chen et al. (1996) and is briefly reviewed here.

The bounding surface model with internal variables is defined in incremental form as either a moment–rotation or a force–displacement relationship and is shown schematically in Fig. 15. Because it is to be calibrated and used with hysteretic force–displacement curves, it takes the form:

Table 2. Hysteretic Properties of Test Specimens

Specimen	Total initial stiffness (kN/mm)	Initial stiffness without BF (kN/mm)	Yield base shear (kN)	Yield displacement (mm)	Maximum drift (%)	μ	Total energy (kN/m)	Energy-infill only (kN/m)
F1	84	73	372	4.6	0.25	1	NA	NA
C1	93	86	518	8	1.4	3	73	50
F2	106	96	364	5.3	3.7	12	444	212

Note: BF=Bounddary Frame, NA=Not Applicable.

Table 3. Bounding Surface Model Parameters

Boundary frame	R_{bf} (kN)	R_b (kN/mm)	h	R_{ki} (kN/mm)	δ_y (mm)	a	b	Error in energy dissipated (%)
BF1	90	3	100	10.64	13.5	0.67	0.42	9.71
BF2	75	3	25	14.46	13.5	0.67	0.42	–3.76

$$\Delta F = R_{kt}\Delta\delta \tag{2}$$

where ΔF=incremental base shear; R_{kt}=tangent stiffness at the current displacement; and $\Delta\delta$=incremental displacement. The tangent stiffness at the current displacement is expressed as

$$R_{kt} = \frac{R_{ki}R_{kp}}{R_{ki} + R_{kp}} \tag{3}$$

where R_{ki}=initial stiffness of the system; and R_{kp}=tangent plastic stiffness at a given displacement and is calculated as

$$R_{kp} = R_b + h\left(\frac{d}{d_{\text{in}} - d}\right) \tag{4}$$

where R_b=slope of the bounding lines with force intercept R_{bf} and is calibrated to asymptotically match the largest displacement excursions in the observed results; h=hardening parameter (used to fit the model to the experimental data); d=distance from the current force to the corresponding bound in the direction of current loading; and d_{in}=value of d at the initiation of loading or at every load reversal. This model is designed to provide curves that asymptotically approach the specified bound lines.

It was found necessary to modify this model slightly in order to capture changes in the initial stiffness of each cycle in which the peak displacement was larger than initial yield displacement. A linear change in initial stiffness with respect to the maximum displacement of a cycle was defined as follows:

$$R_{ki} = R_{kii}a\left(\frac{\delta_{\max}}{\delta_y} + b\right) \tag{5}$$

where R_{kii}=initial stiffness prior to any displacement reaching the yield displacement; a and b=parameters used to fit the experimental data; δ_y=initial yield displacement of the boundary frame; and $\delta_{\max}$=the maximum displacement reached during the next cycle of loading. Additionally, a limit of 2.5 times the initial stiffness (R_{kii}) was placed on R_{ki}.

Figs. 16(a and b) show the experimentally obtained hystereses and the results of the application of the bounding surface model with internal variables described above, for BF1 (the boundary frame used in Specimens F1 and F2) and BF2 (the boundary frame used in Specimen C1), respectively. The values for the parameters used in each model are presented in Table 3, along with the percent error in cumulative energy dissipated (found by numerically integrating both the experimental and modeled data). Note that in both cases the error is less than 10%. The model was implemented in MatLab (MathWorks 1999).

Energy Dissipation by the Infills

Using the model described above, the behavior of the boundary frames could be predicted for the displacement history recorded during the testing of the specimens. The results, superimposed on the hystereses of Specimen C1, and F2, are shown in Figs. 17(a and b), respectively. The boundary frame contributions can then be directly subtracted from the total specimen hystereses, resulting in Figs. 18(a and b), representing the contribution of the infills alone to the hysteretic behavior.

Using the hystereses of the infills only, as well as the total hystereses of the specimens, the values reported in Table 3 were

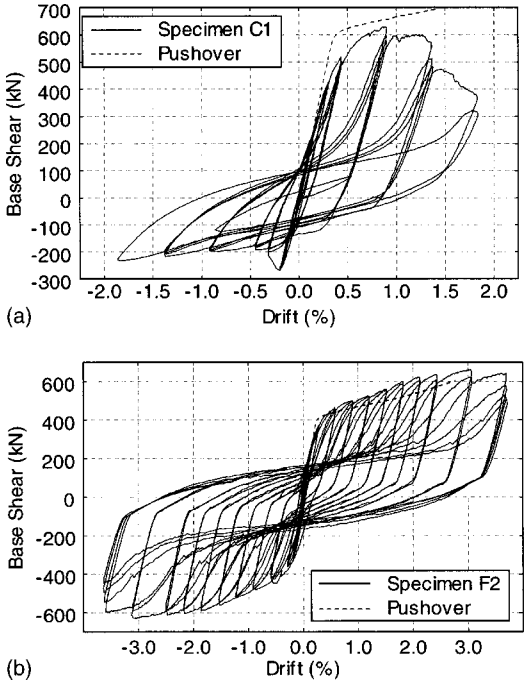

Fig. 10. Specimen hystereses and pushover curves (a) Specimen C1 and (b) Specimen F2

Fig. 11. Global and local buckling of Specimen C1 at $-3\Delta_y$ of Cycle 16

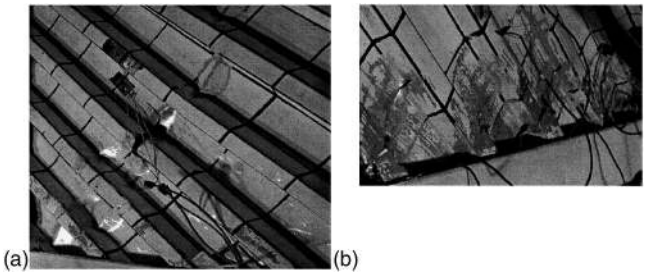

Fig. 12. Examples of infill fractures at $4\Delta_y$ Specimen C1

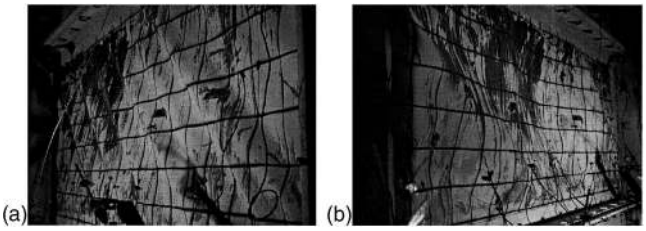

Fig. 13. Infill buckling of Specimen F2:(a) at $6\delta_y$ and (b) at zero load after $6\delta_y$

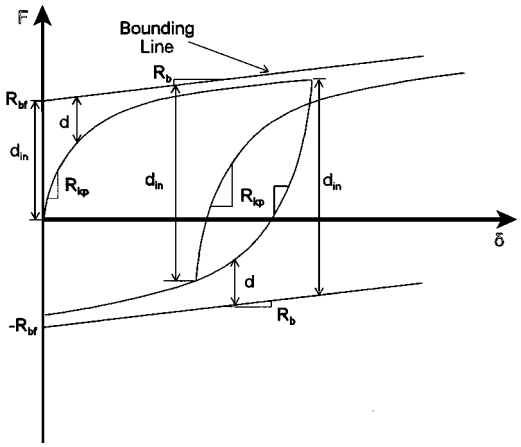

Fig. 15. Schematic of bounding surface model (adapted from Chen et al. 1996)

found. As mentioned before, the initial stiffness of the specimens was largely due to the infills. Furthermore, the energy dissipated by the infills corresponds to 2/3 of the total energy dissipated for Specimen C1 and almost 1/2 the total energy dissipated for Specimen F2. The latter of these two is somewhat misleading due to the large drifts reached by Specimen F2. Fig. 19 shows the cumulative energy dissipated by component for Specimen F2. From this figure, it is apparent that the infill dissipates more than 50% of the total energy dissipated until about Cycle 28, which corresponds to a ductility ratio of 12 and drift of 3.7%. These drifts exceed what would be expected for SPSW during a major

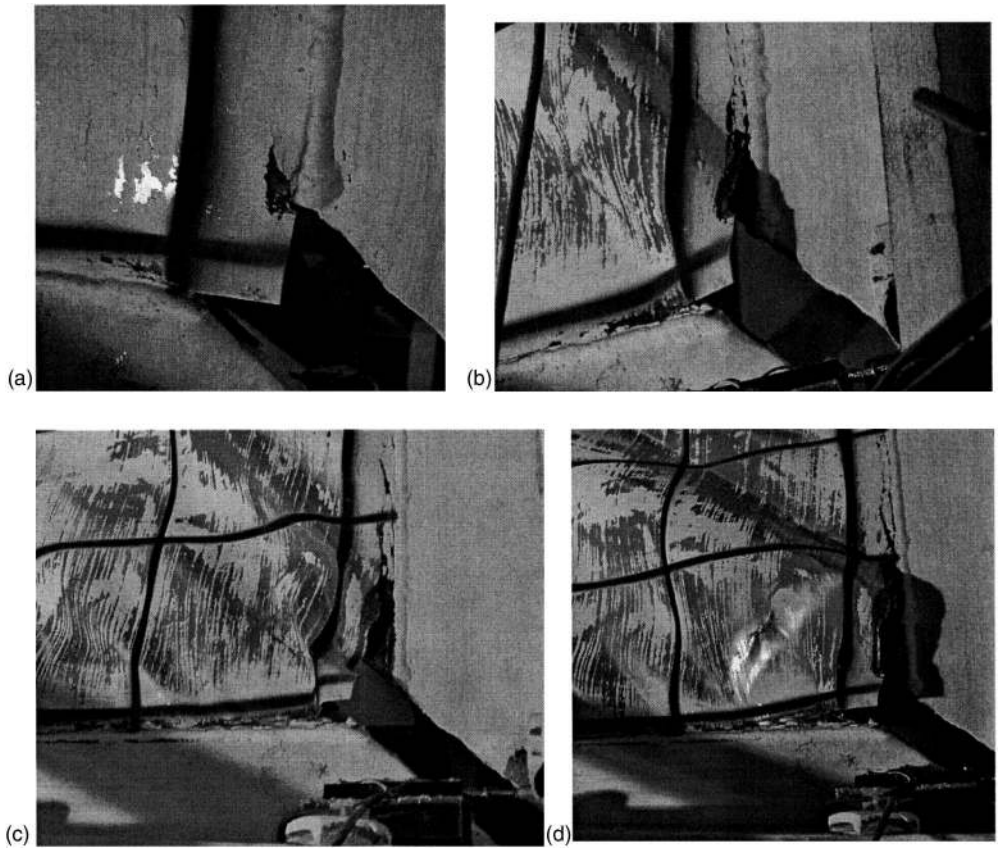

Fig. 14. Fracture propagation-Lower south corner-Specimen F2 (a) $3\Delta_y$; (b) $6\Delta_y$; (c) $8\Delta_y$; and (d) $10\Delta_y$

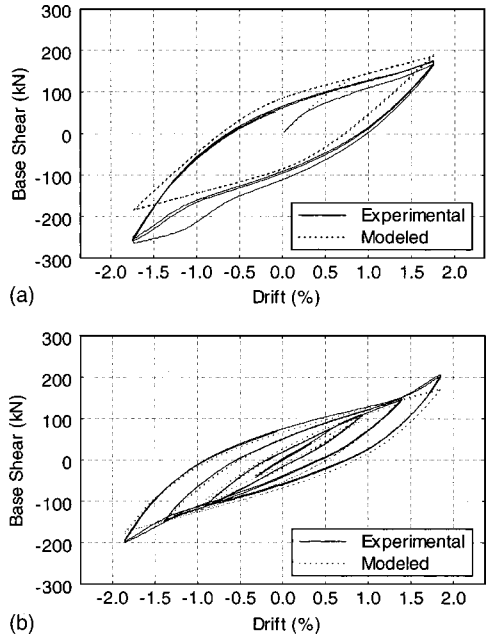

Fig. 16. Experimental and modeled boundary frame hystereses: (a) BF1 and (b) BF2

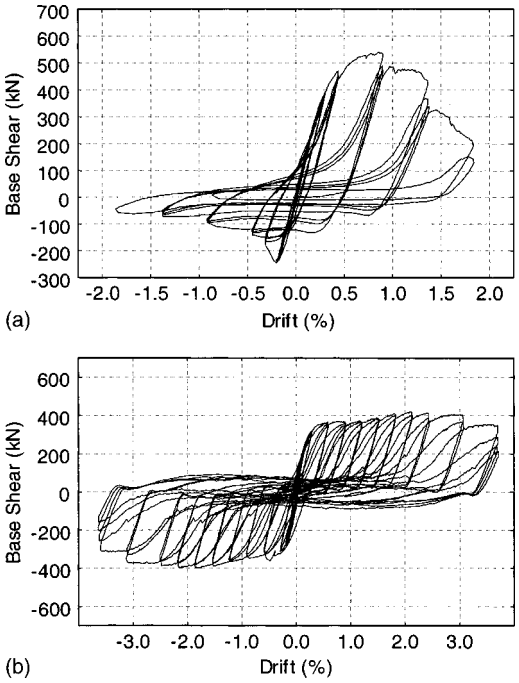

Fig. 18. Infill-only hystereses: (a) Specimen C1 and (b) Specimen F2

seismic event. At drifts of 1.5% (approximately Cycle 19 and $5\Delta_y$), Fig. 19 shows that approximately 2/3 of the hysteretic energy is dissipated by the infill.

Conclusions

Three light-gauge SPSW specimens were designed and tested using quasi-static loading. Two of the specimens had flat infill plates, one with an epoxy connection to the boundary frame and one with a welded connection, while the third was designed with a corrugated infill plate and also utilized an epoxy connection to the boundary frame. Specimen design was based on prototype light-gauge SPSWs, themselves designed as seismic retrofit options for a demonstration hospital. Two of the three specimens were shown to achieve the goals of increased stiffness, energy dissipation capability, and ductility of the existing framing, while using bolted connections detailed in a manner that provides a possibility to relocate the infills elsewhere in the building.

From the experimental results, it was shown that the entire infill of the light-gauge SPSW specimens participated in dissipating energy. Though the hysteretic curves of the specimens were pinched, they were stable and provided significant energy dissipation in the cases of the specimens with the corrugated infill and the flat infill in which the welded connection was used (the former being significantly more ductile). Furthermore, the adequacy of the strip model in predicting the monotonic behavior of light-gauge SPSWs into the nonlinear range was found to be acceptable through comparison with the experimental results.

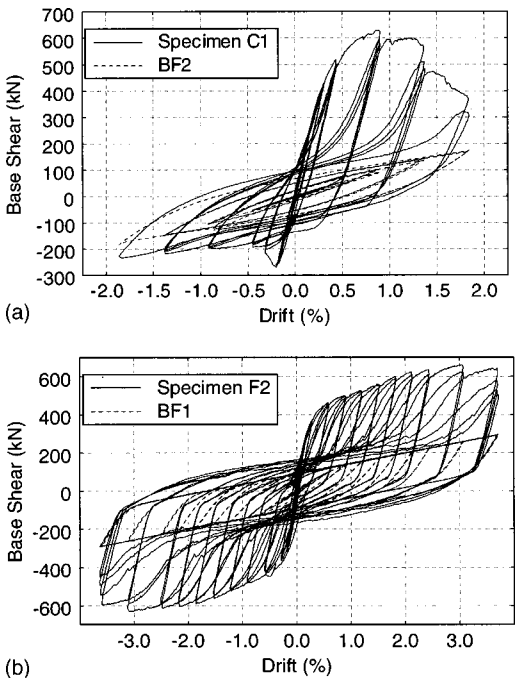

Fig. 17. Specimen and modeled boundary frame hystereses: (a) Specimen C1 and BF2 and (b) Specimen F2 and BF1

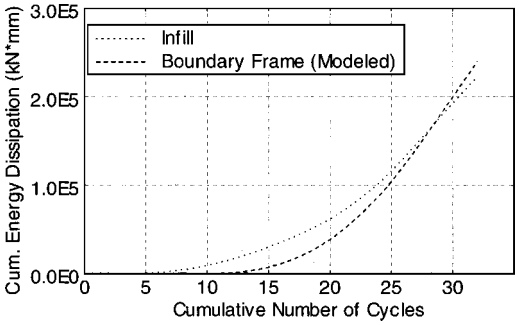

Fig. 19. Energy dissipated by component for Specimen F2

The ultimate failure mode of the specimen which utilized a corrugated infill was found to be fracture of the infill at locations of repeated local buckling and an industrial strength epoxy was found to be an adequate material to connect the infill to the boundary frame in this case. For the specimen using the flat infill and an epoxy connection to the boundary frame, failure occurred in the epoxy prior to yielding of the infill. The specimen utilizing a flat infill and a welded connection to the boundary frame was significantly more ductile than the other two and failure was the result of fractures in the infill adjacent to the fillet weld used to connect the infill to the boundary frame. Despite these fractures near the welded connection, which appeared in the early stages of the test, this specimen did not suffer a significant loss of strength until 12 times the yield displacement.

Acknowledgment

This work was supported in whole by the Earthquake Engineering Research Centers Program of the National Science Foundation under Award No. ECC-9701471 to the Multidisciplinary Center for Earthquake Engineering Research. However, any opinions, findings, conclusions, and recommendations presented in this paper are those of the writers and do not necessarily reflect the views of the sponsors.

References

Applied Technology Council. (ATC). (1992). "Guidelines for seismic testing of components of steel structures." *Rep. No. 24*, ATC, Redwood City, CA 94065.

ASTM. (1997). "Standard specification for commercial steel sheet, carbon, cold-rolled." *A 366/A 336M-97*, American Society for Testing and Materials, Philadelphia.

ASTM. (1998). "Standard specification for steel sheet, zinc-coated (galvanized) zinc-iron alloy-coated (galvannealed) by the hot-dip process." *A 653/A 653M-98*, American Society for Testing and Materials, Philadelphia.

Berman, J. W., and Bruneau, M. (2003a). "Experimental investigation of light-gauge steel plate shear walls for the seismic retrofit of buildings." *Tech. Rep. No. MCEER-03-0001*, Multidisciplinary Center for Earthquake Engineering Research, Univ. at Buffalo, Buffalo, N.Y.

Berman, J. W., and Bruneau, M. (2003b). "Plastic analysis and design of steel plate shear walls." *J. Struct. Eng.*, 129(11), 1148–1156.

Bruneau, M., Uang, C. M., and Whittaker, A. (1997). *Ductile design of steel structures*, McGraw-Hill, N.Y.

Caccese, V., Elgaaly, M., and Chen, R. (1993). "Experimental study of thin steel-plate shear walls under cyclic load." *J. Struct. Eng.*, 119(2), 573–587.

Canadian Standards Association (CSA). (2001). "Limit states design of steel structures." *CAN/CSA S16-01*, Willowdale, Ontario, Canada.

Chen, W. F., Goto, Y., and Liew, J. Y. R. (1996). *Stability design of semirigid frames*, Wiley, N.Y.

Cook, N. E. (1983). "Strength of flexibly-connected steel frames under load histories." PhD dissertation, Univ. of Colorado—Boulder, Boulder, Colo.

Dafalias, Y. F., and Popov, E. P. (1976). "Plastic internal variables formalism of cyclic plasticity." *J. Appl. Mech.*, 43, 645–651.

Driver, R. G., Kulak, G. L., Kennedy, D. J. L., and Elwi, A. E. (1997). "Seismic behavior of steel plate shear walls." *Structural Engineering Rep. No. 215*, Dept. of Civil Engineering, Univ. of Alberta, Edmonton, Alberta, Canada.

Elgaaly, M., Caccese, V., and Du, C. (1993). "Postbuckling behavior of steel-plate shear walls under cyclic loads." *J. Struct. Eng.*, 119(2), 588–605.

Federal Emergency Management Agency (FEMA). (1997). "NEHRP Recommended Provisions for Seismic Regulations for New Buildings and Other Structures, Part-1-Provisions." *FEMA 302*, Building Seismic Safety Council for the FEMA, Washington, D.C.

Goto, Y., Suzuki, S., and Chen, W. F. (1991). "Analysis of critical behavior of semirigid frames with or without load histories in connections." *Int. J. Solids Struct.*, 27(4), 467–483.

Loctite. (2001). "Product description sheet-Hysol product 9460." Loctite Inc., Rocky Hill, Conn.

MathWorks. (1999). *MatLab Function Reference*, The MathWorks, Inc., Natick, Mass.

Rezai, M. (1999). "Seismic behavior of steel plate shear walls by shake table testing." PhD dissertation, Univ. of British Columbia, Vancouver, British Columbia, Canada.

Thorburn, L. J., Kulak, G. L., and Montgomery, C. J. (1983). "Analysis of steel plate shear walls." *Structural Engineering Rep. No. 107*, Dept. of Civil Engineering, Univ. of Alberta, Edmonton, Alberta, Canada.

Timler, P. A., and Kulak, G. L. (1983). "Experimental study of steel plate shear walls." *Structural Engineering Report No. 114*, Dept. of Civil Engineering, Univ. of Alberta, Edmonton, Alberta, Canada.

Yang, T. Y., and Whittaker, A. (2002). "MCEER demonstration hospitals-Mathematical models and preliminary results." *Tech. Rep.*, Multidisciplinary Center for Earthquake Engineering Research, Univ. at Buffalo, Buffalo, N.Y.